THE JOURNAL OF BIOLOGICAL CHEMISTRY VOL. 286, NO. 29, pp. 26016–26027, July 22, 2011

Adamts5 Deletion Blocks Murine Dermal Repair through CD44-mediated Aggrecan Accumulation and Modulation of Transforming Growth Factor β1 (TGFβ1) Signaling*[S]

Received for publication, December 2, 2010, and in revised form, April 27, 2011 Published, JBC Papers in Press, May 12, 2011, DOI 10.1074/jbc.M110.208694

Jennifer Velasco[‡], Jun Li[§], Luisa DiPietro[¶], Mary Ann Stepp[‖], John D. Sandy[‡], and Anna Plaas[‡§1]

From the Departments of [‡]Biochemistry and [§]Internal Medicine (Rheumatology), Rush University Medical Center, Chicago, Illinois 60612, the [¶]Center for Wound Repair and Regeneration, College of Dentistry, University of Illinois, Chicago, Illinois 60612, and the [‖]Department of Anatomy and Regenerative Biology, George Washington University Medical School, Washington, D. C. 20037

ADAMTS5 has been implicated in the degradation of cartilage aggrecan in human osteoarthritis. Here, we describe a novel role for the enzyme in the regulation of TGFβ1 signaling in dermal fibroblasts both *in vivo* and *in vitro*. *Adamts5*$^{-/-}$ mice, generated by deletion of exon 2, exhibit impaired contraction and dermal collagen deposition in an excisional wound healing model. This was accompanied by accumulation in the dermal layer of cell aggregates and fibroblastic cells surrounded by a pericellular matrix enriched in full-length aggrecan. *Adamts5*$^{-/-}$ wounds exhibit low expression (relative to wild type) of collagen type I and type III but show a persistently elevated expression of tgfbRII and alk1. Aggrecan deposition and impaired dermal repair in *Adamts5*$^{-/-}$ mice are both dependent on CD44, and *Cd44*$^{-/-}$/*Adamts5*$^{-/-}$ mice display robust activation of TGFβ receptor II and collagen type III expression and the dermal regeneration seen in WT mice. TGFβ1 treatment of newborn fibroblasts from wild type mice results in Smad2/3 phosphorylation, whereas cells from *Adamts5*$^{-/-}$ mice phosphorylate Smad1/5/8. The altered TGFβ1 response in the *Adamts5*$^{-/-}$ cells is dependent on the presence of aggrecan and expression of CD44, because *Cd44*$^{-/-}$/*Adamts5*$^{-/-}$ cells respond like WT cells. We propose that ADAMTS5 deficiency in fibrous tissues results in a poor repair response due to the accumulation of aggrecan in the pericellular matrix of fibroblast progenitor cells, which prevents their transition to mature fibroblasts. Thus, the capacity of ADAMTS5 to modulate critical tissue repair signaling events suggests a unique role for this enzyme, which sets it apart from other members of the ADAMTS family of proteases.

Dermal wound healing involves a series of cellular responses that depend on the coordinated temporal and spatial expression of inflammatory cytokines, proteases, growth factors, and extracellular matrix molecules. The early phases of hemostasis, inflammation, and re-epithelialization are followed by granulation tissue formation and finally dermal remodeling (1, 2). The granulation tissue is a loosely organized collagenous matrix that serves as a template for cellular regeneration (3) of the collagen (4) and proteoglycan (5–7) structures of the dermis proper.

There has been a long held consensus that proteinases, such as plasmin and matrix metalloproteinases, are major players in dermal repair; however, many questions remain regarding substrate and product identification and to what extent cleavage of particular proteins is destructive or reparative (reviewed in Ref. 8). Although much interest has focused on matrix metalloproteinases (9), the ADAMTSs have now also been found to play a major role in a range of repair and regeneration processes. For example, evidence of a role for ADAMTS activity in dermal repair comes from the finding that human skin contains abundant aggrecanase-generated catabolic fragments of versican V0 and V1 (5) and that both aggrecan and versican are associated with the dermal region of the hair follicle (7). Moreover, to place dermal matrix turnover in a broader context, cleavage of the hyalectans aggrecan, versican, and brevican by one or more aggrecanases (ADAMTS1, -4, -5, -8, -9, and -15) occurs in the remodeling of cartilage (10), aorta (11, 12), spinal cord (13), meniscus (14, 15) intervertebral disc (16), adipose tissue (17), and brain (18).

HA[2] in the skin is most abundant in the epidermal layer (6), and it undergoes partial fragmentation in both the dermis and epidermis of human skin explants (19). Its role in skin biology has largely focused on its binding to the cell-surface receptor CD44, an interaction that prevents PDGF-BB receptor activation and human fibroblast migration (20). It also appears to be required for MMP9-mediated activation of TGFβ1 (21). HA has been shown to ligate RHAMM to promote the association of CD44 and p-ERK, an interaction that directly activates cell migration and thereby is required for efficient dermal repair (22, 23). HA also regulates the proliferative response of dermal fibroblasts to TGFβ1 (24), and HA12 oligosaccharides stimulate Col3 and TGFβ1 expression (25), a finding that is very relevant to the data described here.

TGFβ1 is a key regulator of multiple processes in dermal wound healing (26). In the context of this study, TGFβ1 stimulates col1 and col3 production by fibroblasts and is required for terminal differentiation of myofibroblasts during wound

* This work was supported, in whole or in part, by National Institutes of Health Training Grant AR007590 (to J. V.). This work was also supported by the Katz/Rubschlager Endowment for OA Research and the Rush Arthritis Institute, Rush University Medical Center (to A. P. and J. D. S.).

[S] The on-line version of this article (available at http://www.jbc.org) contains supplemental Figs. S1–S8 and Tables S1 and S2.

[1] To whom correspondence should be addressed. Tel.: 312-942-7194; Fax: 312-942-3053; E-mail: anna_plaas@rush.edu.

[2] The abbreviations used are: HA, hyaluronan; col1, collagen type I; col3, collagen type III; ECM, extracellular matrix.

contracture (27). Furthermore, the pro-fibrotic effects of TGFβ1 on both normal and scleroderma skin-derived fibroblasts require signaling through ALK5 and phosphorylation of Smad2/3 (28, 29). We have recently shown that TS5-mediated cleavage of aggrecan is required for the pro-fibrotic responses of synovium, meniscus, and cartilage in murine models of osteoarthritis (30) and also the fibrogenic phase of ligament repair in equine degenerative suspensory ligament desmitis (31). Therefore, this study was undertaken to further elucidate a mechanism by which TS5-mediated cleavage of aggrecan is required for the fibrotic response of reparative cells to stimuli such as TGFβ1. For this purpose, we chose to examine the role of TS5 in the established excisional dermal wound healing model, and to compare the progression of granulation tissue formation, re-epithelialization, contracture, and dermal remodeling in WT and *ts5*$^{-/-}$ mice. The data presented here confirmed the role of the enzyme in contracture and dermal remodeling. Thus, in the absence of TS5, the pericellular accumulation of CD44-bound HA-aggrecan on fibroblast progenitor cells promotes their assembly into cell aggregates with an epithelioid morphology that disrupts the reforming dermis. Mechanistic studies with isolated fibroblasts show that pericellular accumulation of aggrecan, due to the absence of TS5, results in an altered TGFβ1 response, including decreased pro-fibrotic signaling through Smad2/3 and increased signaling through Smad1/5/8.

EXPERIMENTAL PROCEDURES

Animal Studies—The protocol was approved under IACUC guidelines at Rush University Medical Center. All mice were on the C57Bl6 background and were bred in-house. The *ts5*$^{-/-}$ line was established by deletion of exon 2, as described previously (32). The *Cd44*$^{-/-}$ line was obtained from The Jackson Laboratory, and the *Cd44*$^{-/-}$/*ts5*$^{-/-}$ double knock-out line was established from heterozygous breeding pairs. Congenic breeding colonies (three breeding pairs) were established for each of the four strains, and littermates from those breeding pairs were used for all experiments described in this study.

Excisional Dermal Wound Healing Model—Male mice at 6 weeks of age were anesthetized, and four excisional wounds were made with a sterile 3-mm biopsy punch (Acuderm, Inc.) on the dorsal skin of each mouse. Wounds were left open to heal, and cages were changed daily to prevent wound contamination.

Macroscopic and Microscopic Evaluation of Dermal Wound Repair—Unwounded mice and mice at 4, 6, 8, and 15 days post-wounding were euthanized and dorsal skins removed. The dermal flap (about 4 cm^2) was excised and placed on PBS-soaked gauze pads on ice. Subdermal and epidermal sides of wounds were immediately photographed under a Nikon dissection microscope (SMZ1000) at ×4 magnification and images were processed with Spot Basic (Diagnostic Instruments, Inc.). The dermal flaps were then secured flat in biopsy bags, fixed with 10% neutral buffered formalin for 3 days, and processed. Five-micron sections were cut and stained with Masson's trichrome staining (Electron Microscopy Sciences, Hatfield, PA) according to the manufacturer's instructions. Confocal immunohistochemistry was performed essentially as described previously (33). Briefly, sections were deparaffinized and incubated with 1 μg/ml of affinity-purified antibody, α-DLS, to detect aggrecan (33), rabbit IgG for nonimmune control (supplemental Fig. S2), ab1033 for versican β-GAG domain (Abcam), or biotinylated aggrecan-G1 domain for hyaluronan (supplemental Fig. S3). Antibody-probed sections were incubated with biotinylated goat anti-rabbit IgG, and bound complexes were visualized with AlexaFluor 594-streptavidin. Nuclei were stained with Sytox Green (1:300 dilution) (Invitrogen) for 15 min at room temperature. ×10 or ×40 images were taken on a Nikon Eclipse TE2000-S inverted confocal microscope, and overlays were generated with MetaMorph software.

Quantitative Real Time PCR Analyses—Dorsal skins were removed and rapidly frozen by expansion on the surface of dry ice. Wounds were excised with a 3-mm dermal punch, rigorously excluding unwounded tissue, placed in liquid nitrogen, and pulverized in a Bessman tissue pulverizer. Four wounds from one mouse were combined for each RNA sample, and five mice from all four genotypes were used for each time point. RNA was prepared using the PerfectPure RNA kit for fibrous tissue (5 PRIME). cDNA synthesis was performed with the SuperScript First-Strand Synthesis System for RT-PCR (Invitrogen) with 1 μg of RNA. The following primers were purchased from Applied Biosystems, Inc.: *aggrecan* (Mm00545794_m1); *alk1* (Mm00437432_m1); *alk5* (Mm00436964_m1); *adamts4* (Mm00556068_m1); *adamts5* (Mm01344180_m1); *cd44* (Mm01277163_m1); *gapdh* (Mm99999915_g1); *versicanV0* (AI7ZZKW); *versicanV1* (Mm00490173_m1); *collagen1a* (Mm00468761_m1); *collagen3a* (Mm00802331_m1); *tgfβ1* (Mm00441724_m1); and *tgfβ1RII* (Mm00436978_m1). Primers were combined with Taqman Gene Expression Master Mix (Applied Biosytems, Inc) and cDNA (diluted 1:10 in diethylpyrocarbonate water). Amplification reactions were performed with a Bio-Rad RT-PCR CFX96 instrument using the following cycling conditions: 50 °C for 2 min, 95 °C for 10 min, 95 °C for 15 s, and 60 °C for 1 min. The cycle was repeated 40–45 times, and the Δ*Ct* data (*Ct* for gene of interest minus *Ct* for internal control, *gapdh*) for each gene at each time point in each genotype were determined. We next processed the Δ*Ct* data using the approach described previously for determining the ratio of mRNA abundance of two different genes in a single sample (52). In this case, we determined the mRNA abundance of a single gene at multiple time points in four genotypes, normalized to the abundance of the same gene in the unwounded WT sample. This means that for any Δ*Ct* value (at any time point), the value was reduced by the Δ*Ct* value for the unwounded WT sample to generate a ΔΔ*Ct* value, and the mRNA abundance was calculated as $2^{-\Delta\Delta Ct}$ (arbitrary units) (Figs. 7 and 8). The same calculations were repeated for each of the eight genes studied.

Western Blot of Aggrecan and Versican in Unwounded and Wounded Skin—Mice were euthanized unwounded and at days 4, 6, 8, and 15 post-wound, and tissue was harvested as described above. Four wounds from each mouse were pooled and placed in PBS buffer with protease inhibitors (10 mM MES, 50 mM sodium acetate, 5 mM EDTA, 0.1 mM 4-(2-aminoethyl)-benzenesulfonyl fluoride, 5 mM iodoacetic acid) on ice for 30 min. Tissues were then snap-frozen in liquid nitrogen, pulver-

ized in a Bessman tissue pulverizer, and extracted in 1 ml of 4 M guanidine HCl, 50 mM sodium acetate, pH 6.8, containing protease inhibitors, on a rocker at 4 °C overnight. Tissue residues were removed by centrifugation at 13,000 rpm for 15 min. Supernatants were dialyzed for 5 h against distilled H_2O, adjusted to 7 M urea, 50 mM Tris acetate, pH 8.0, and proteoglycans were purified by DE52 ion exchange chromatography as described previously (34, 35). Samples were extensively dialyzed against water, speedvac dried, redissolved in 5 mM Tris acetate, 10 μM EDTA, pH 7.6, and digested with proteinase-free chondroitinase ABC. SDS-PAGE and Western blotting were performed as described previously (31, 33) using α-DLS (0.5 μg/ml), α-NITEGE (0.5 μg/ml), or α-G1 for aggrecan, ab1033 (1:2000) for versican β-GAG domain, and α-DPE for the aggrecanase-generated G1 domain product of versican V0/V1(37). α-DLS was raised in rabbits by injection of the peptide CGGSGVEDLS linked to keyhole limpet hemocyanin. In mouse aggrecan, this sequence was found in the CS-1 domain at DLS sequences with serine residues at positions 969, 709, and 1206. Proteoglycans were isolated from three mice at each time point for all genotypes. Extracts from each individual mouse were analyzed separately, and gels shown are representative of the three separate analyses.

Newborn Skin Fibroblast Cultures—Cells were isolated and cultured essentially as described previously (38). Briefly, 4–6 pups (24–48 h old) were euthanized in a CO_2 chamber for 20 min, cleaned with betadine, rinsed with deionized water, and briefly immersed in 70% alcohol. Skins were removed, transferred to 10 ml of cold 0.25% trypsin in Ca^{2+}/Mg^{2+}-free Hanks' buffered saline solution (Mediatech, Inc.) with the skin floating on the enzyme solution, and incubated for 18 h at 4 °C. The dermis was separated from the epidermis, rinsed with PBS, and digested with 0.35% collagenase (Worthington) in DMEM (Mediatech, Inc.) at 37 °C for 30 min in a shaking incubator. Released cells were filtered through a 70-μm cell sieve (BD Biosciences) to remove undigested fragments, recovered by centrifugation, and finally suspended in DMEM, 10% FBS/FetalClone III (Hyclone), 100 units/ml penicillin, 100 μg/ml streptomycin, 10 μg/ml gentamycin, 0.25 μg/ml fungizone, and 2 mM L-glutamine at 1×10^4 cells/ml, and 20 ml plated in T-75 flasks (Corning). Cells were grown to confluence, then subcultured using 0.25% trypsin/EDTA solution (Mediatech, Inc.), and split at a 1:3 ratio. All experiments were performed in 100-mm dishes (Corning Glass) on confluent 3rd passage cells. Western analysis of aggrecan in WT and $ts5^{-/-}$ fibroblast cultures showed that the $ts5^{-/-}$ cells accumulated by far the most full-length product, as detected by α-DLS or α-G1 (supplemental Fig. S6*A*), whereas the WT cells accumulated more of the proteolytically processed G1-reactive species at about 120 and 70 kDa (also reactive with α-NITEGE, see supplemental Fig. S6*B*).

TGFβ1 Treatment of Skin Fibroblasts—Cells were incubated in medium containing 0.1% serum for 18 h and replaced with fresh medium containing 10 ng/ml TGFβ1 (human recombinant, PeproTech Inc.). Cultures were terminated at different times by a brief wash with PBS and followed by extraction on a rocking platform for 1 h at 4 °C with 250 μl of mammalian protein extraction reagent (M-PER, Thermo Scientific), including protease inhibitor mixture (Sigma), and phosphatase inhibitor 1 and 2 (Sigma) at 1:100 dilution each. These cell lysates were centrifuged at 14,000 rpm for 15 min at 4 °C to clarify samples and supernatants stored at −20 °C until Western blot analyses.

Streptomyces Hyaluronidase Treatment of Skin Fibroblasts—Medium was removed from fibroblast cultures and replaced with PBS containing 20 units/ml enzyme (Seikagaku Inc.), and after 20 min at 37 °C, the released products were removed, and the cell layers were extracted with 500 μl of isotonic salt extraction solution (50 mM Tris-HCl, 150 mM NaCl, 5 mM EDTA, 0.5% Nonidet P-40). Proteoglycans were purified by DE52 chromatography for digestion with chondroitinase ABC (PF) and Western analysis.

Western Analysis of Smad2, Smad3C, and Smad1/5/8—The total protein content in cell extracts was determined using the BCA protein assay kit (Pierce). Portions containing 5 μg of protein were dried by speedvac and suspended in 20 μl of sample buffer (Novex 2× Tris glycine SDS Sample Buffer, 6 M urea, 25 mg/ml DL-dithiothreitol) heated at 100 °C for 5 min, and electrophoresed on 4–12% Tris glycine gels (Invitrogen). Separated proteins were blotted to nitrocellulose membranes and reacted with the following antibodies (all from Cell Signaling): α-pSmad2 1:1000; α-pSmad3C 1:1000; α-Smad2/3 1:1000; α-pSmad1/5/8 1:1000, and α-Smad1 1:1000. Millipore ECL reagents were used to develop the membranes. All Smad blots were exposed for 1 min and pSmad blots for 5 min. Band intensities were determined as Integrated Pixel Densities using ImageJ software (National Institutes of Health).

RESULTS

$Adamts5^{-/-}$ Mice Exhibit Abnormal Repair of the Collagenous Dermal Matrix following Excisional Wounding—Wound healing progression was monitored by photography of the subdermal and epidermal surfaces at the following times: day 4 (granulation tissue formation/re-epithelialization), day 8 (wound contraction and fibroblast maturation), and day 15 (dermal collagen network regeneration). In WT mice (Fig. 1*A*, *left panels*), inflammation and vascularization around excised wound sites were maximum at day 4 and completely resolved by day 15. The expected time course of re-epithelialization, contraction, and complete closure with re-growth of hair was also evident at this time. Conversely, whereas $ts5^{-/-}$ mice showed a normal inflammatory and vascularization response at day 4 (Fig. 1*B*, *left panels*), these responses did not recede on days 8 and 15. Whereas the epidermal scab was formed on day 4, the wounds had not contracted even by day 15, leading to ulceration with poor hair growth. This difference in healing responses between WT and $ts5^{-/-}$ mice was also examined histologically by Masson Trichrome staining (Fig. 1, *A* and *B*, *right hand panels*; high magnification image in supplemental Fig. S1). This confirmed granulation tissue formation at day 4, which was replaced in WTs by dense collagen fibrillar dermis. In $ts5^{-/-}$ mice, by contrast, at both days 8 and 15, the collagenous matrix in the dermis was less dense, and most notably, cell aggregates, which resemble regenerating hair follicles, were abundant, even in the lower regions of the regenerating dermis (Fig. 1*B*, histology, *black arrows*). The expression of ts4, ts5, and cd44 in WT mice (supplemental Fig. S5) showed enhancement

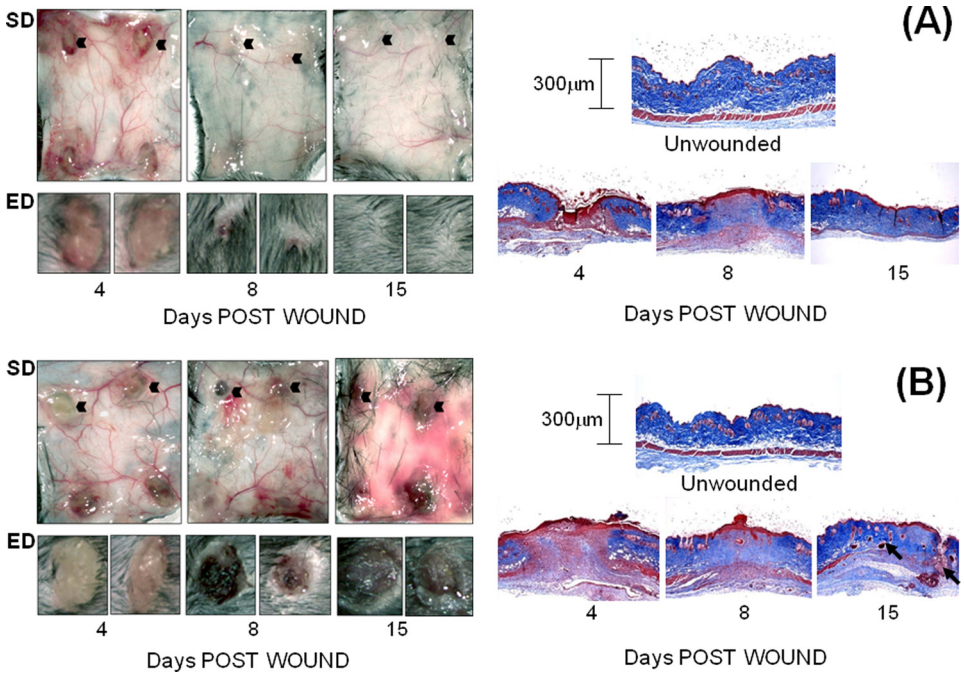

FIGURE 1. **Macroscopic view of dermal and epidermal wound closure in WT (*A*) and *ts5*$^{-/-}$ (*B*) mice.** Four 3-mm wounds were made on the dorsal skin of mice that were sacrificed at 4, 8, and 15 days post-wounding. *Left-hand panels* show the macroscopic appearance of the dermal skin flap on the subdermal side (*SD*) to illustrate vascularization and inflammatory responses. The epidermal (*ED*) view of two representative wounds (indicated by *black arrowhead*) is also shown. *Right-hand panels* show representative histological sections after Mason trichrome staining of unwounded skin and wounds at 4, 8, and 15 days. Size bars for histology are given in the *right-hand panels*.

at day 8, consistent with a role for these components in the contraction and regeneration phases.

Accumulation of Aggrecan, Versican, and Hyaluronan in Cell Aggregates in the Regenerating Dermis of ts5$^{-/-}$ *Mice*—Western analyses for aggrecan and versican on wound extracts from both genotypes (Fig. 2) were done to examine if the repair deficiencies in the *ts5*$^{-/-}$ mice were accompanied by the accumulation of uncleaved substrates, such as aggrecan and versican (25). Aggrecan was barely detectable in unwounded WT skin; it increased markedly at day 4 during granulation tissue formation and returned to the low level of unwounded skin during the contraction phase (Fig. 2*A*). Unwounded *ts5*$^{-/-}$ skin (Fig. 2*B*) was also low in aggrecan, but there was no significant accumulation during the granulation phase. However, in contrast to WT, the *ts5*$^{-/-}$ wounds accumulated aggrecan throughout the contraction and dermal regeneration phases (Fig. 2*B*). The aggrecan core species for both genotypes migrated as a broad band, mostly above the 250-kDa marker. Aggrecan accumulation following skin wounding was repeated in two other experiments (supplemental Fig. S4), and the results supported the general theme of *ts5*$^{-/-}$ mice accumulating abundant dermal aggrecan relative to WT.

Analysis of these same post-wound samples for versican with Ab1033 to the β-GAG domain, showed very little deposition in WT wounds (Fig. 2*A*) but marked accumulation in *ts5*$^{-/-}$ wounds (Fig. 2*B*), particularly at day 8, and notably, this was followed by its removal by day 15. *ts5*$^{-/-}$ wounds contained at least five core species with approximate sizes of 140, 110, 90, and 60 kDa. Analysis with and without chondroitinase showed that these were present largely in chondroitin sulfate-substituted forms. Whereas the precise structure of these species is unknown, they are most likely all derived from the V1 isoform, as analyses of the same samples with Ab1032 for α-GAG domain in V0 (data not shown) gave no reactivity. WT skin and wounds (Fig. 2*A*) contained very little versican, and this was largely the 90-kDa species predominantly in the chondroitin sulfate-unsubstituted form. Western analysis of these samples with α-DPE (supplemental Fig. S6) showed that the 90-kDa product in the WT and *ts5*$^{-/-}$ extracts was the murine equivalent of the 90-kDa human dermal versican V1 product, previously identified as the ADAMTS-aggrecanase generated G1-DPEAAE441 (37). It should be noted that minor differences in electrophoretic migration properties of core protein species were noted between the different strains (for example compare WT and *ts5*$^{-/-}$ in Fig. 2, *A* and *B*, with *Cd44*$^{-/-}$ in Fig. 6, *A* and *B*). Such differences could be explained by differential extracellular proteolysis and/or variable glycosylation that affect electrophoretic properties of the chondroitinase-generated core proteins.

Confocal localization of aggrecan versican and hyaluronan showed that in unwounded skin of both WT and *ts5*$^{-/-}$ mice, all three were present in the ECM surrounding epithelial cells and also cells lining hair follicles and sweat glands (Fig. 3 and supplemental Fig. S3). At day 4 (granulation phase), WT wounds accumulated abundant aggrecan, but this was much reduced in TS5$^{-/-}$ wounds, in keeping with the Western data in Fig. 2. During this phase, both versican and hyaluronan were detected largely in the scabs for both genotypes (supplemental Fig. S3). After day 8, in WT wounds, minor staining for aggrecan was detectable in the newly formed epidermis, appendages, and in subdermal blood vessels (Fig. 4, *A* and *B*, *upper panels*). In *ts5*$^{-/-}$ late stage wounds, aggrecan was also abundant in the

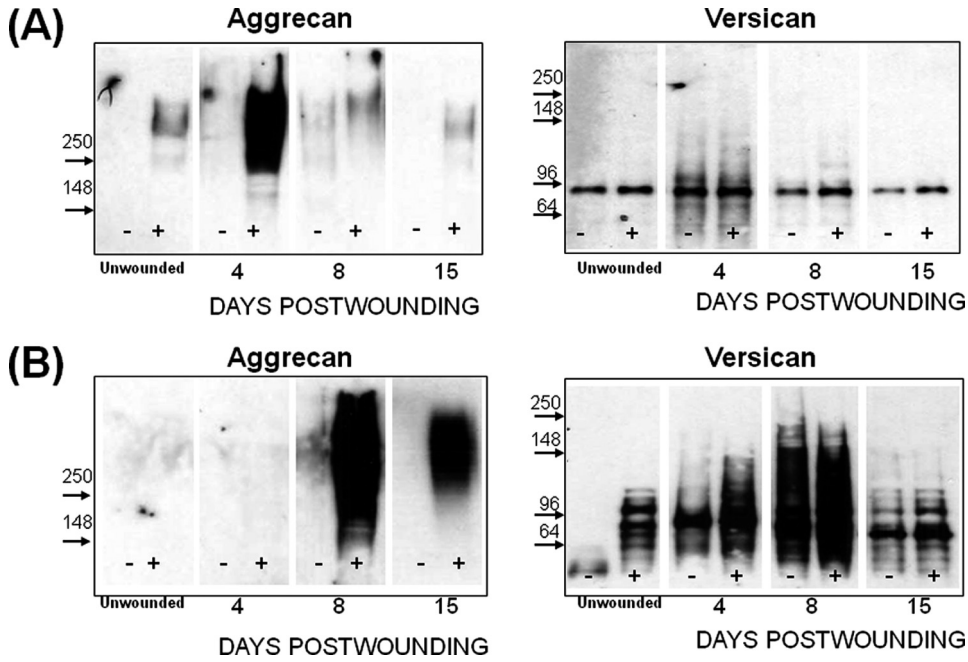

FIGURE 2. **Aggrecan and versican deposition in regenerating skin of WT (*A*) and *ts5*$^{-/-}$ (*B*) mice.** Proteoglycans were prepared for Western analysis with anti-aggrecan (α-DLS) and with anti-versican V1 (Ab1033). Each lane was loaded with 20% of the proteoglycan-rich fraction isolated from the four wound sites combined from one mouse. Samples loaded without and with chondroitinase ABC digestion are marked − and +, respectively. Images separated by dividing lines were from different parts of the same gel. (Also see supplemental Fig. S4 for more data.)

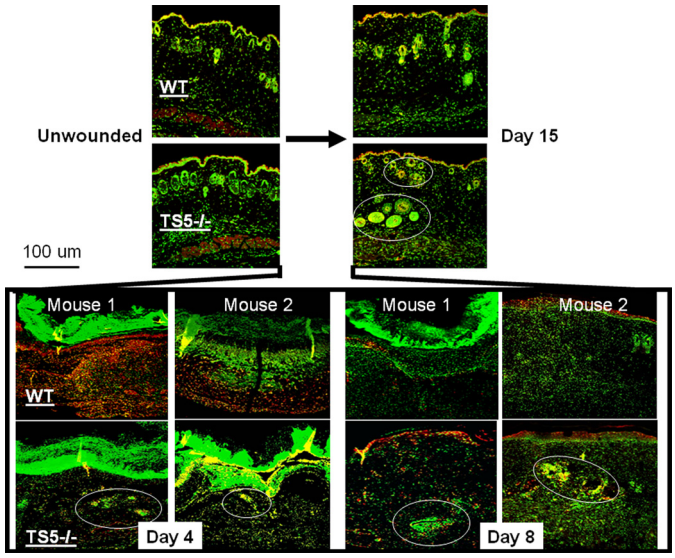

FIGURE 3. **Localization of aggrecan in unwounded skin and 4, 8, and 15 days post-wounding from WT and *ts5*$^{-/-}$ mice.** Sections were stained for confocal microscopy as described under "Experimental Procedures." Images shown were taken under ×10 magnification. *Green fluorescence,* nuclei; *red fluorescence,* aggrecan; *yellow,* intracellular or pericellular aggrecan. Aggrecan-+ve cell aggregates in *ts5*$^{-/-}$ wounds are shown by *white circles*. Also see supplemental Fig. S2 for nonimmune controls. *Size bar,* 100 μm.

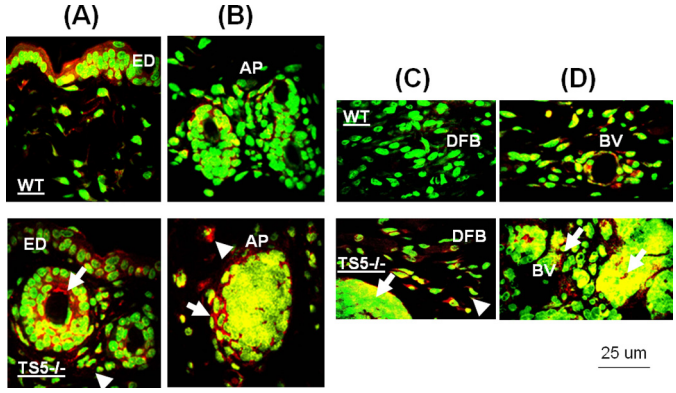

FIGURE 4. **Localization of aggrecan in epidermal and dermal layers of *ts5*$^{-/-}$ and WT mice at 15 days post-wounding.** Sections were stained as described under "Experimental Procedures" and viewed at ×40 to show the epidermal layer (*ED*) (*A*), newly formed skin appendages beneath the epidermal layer (*B*), dermal fibroblasts (*DFB*) (*C*) , and subdermal blood vessels (*BV*) (*D*). *AP,* skin appendages. The accumulation of aggrecan in cell aggregates and fibroblasts in *ts5*$^{-/-}$ mice only is shown by *white arrowheads*. *Green fluorescence,* nuclei; *red fluorescence,* aggrecan; *yellow,* intracellular or pericellular aggrecan. *Size bar,* 25 μm size. Also see supplemental Fig. S3 for versican and hyaluronan localization in *ts5*$^{-/-}$ cell aggregates.

newly formed epithelial layer and appendages and was also present within the pericellular space surrounding cell aggregates that were distributed throughout the nonhealing dermis (Fig. 4, *A* and *B, lower panels*). These cell aggregates in *ts5*$^{-/-}$ wounds were also positive for versican and hyaluronan (supplemental Fig. S3). Most strikingly, however, the fibroblastic cells throughout the dermis of the *ts5*$^{-/-}$ mice only showed robust cell-associated aggrecan staining (Fig. 4, *A–D, white arrows*).

It was noted that a proportion of all three ECM molecules co-localized with the nuclear stain, suggesting intracellular localization. Further work is required to determine whether this represents localization in the nucleus or intracellular organelles (such as endosomes or phagosomes) that may have "collapsed" into a perinuclear region due to the fixation and processing techniques used here.

Aggrecan Accumulation during Dermal Wound Healing Is Dependent on the Presence of CD44—It is widely recognized (39) that immature hair follicles, such as those seen abundantly in *ts5*$^{-/-}$ regenerating dermis (Fig. 4), contain pluripotent cells that represent a major source for the fibroblasts required for

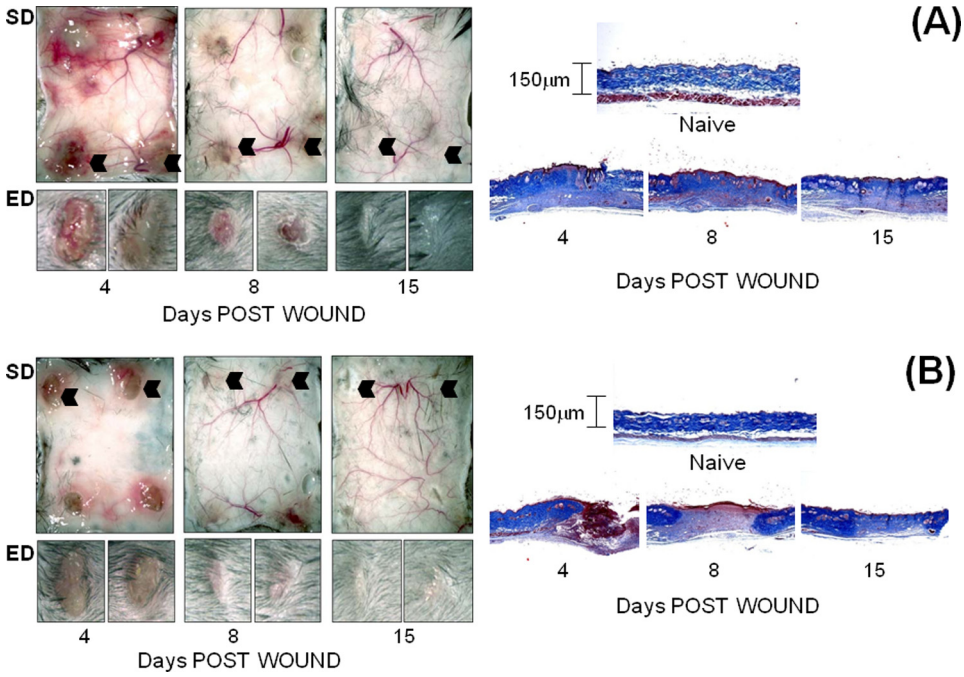

FIGURE 5. **Macroscopic view of dermal and epidermal wound closure in $Cd44^{-/-}/ts5^{-/-}$ (*A*) and $Cd44^{-/-}$ (*B*) mice.** Four 3-mm wounds were made on the dorsal skin of mice that were sacrificed at 4, 8, and 15 days post-wounding. *Left-hand panels* show the macroscopic appearance of the dermal skin flap on the subdermal side (*SD*) to illustrate vascularization and inflammatory responses. The epidermal (*ED*) view of two representative wounds (indicated by *black arrowhead*) is also shown. *Right-hand panels* show representative histological sections after Mason trichrome staining of unwounded skin and wounds at 4, 8, and 15 days. *Size bars* for histology are given in the *right-hand panels*.

dermal repair. This suggested that the cell aggregates seen here might be related to the condensed mesenchymal groups, which have been extensively studied as precursors for overt cartilage formation during limb development (40). In this context, the condensation of such cell groups has been shown to depend on CD44-mediated binding of hyaluronan to cell surfaces (40). Therefore, to investigate the possibility that CD44 is required for matrix stability around the abnormal cell aggregates in regenerating dermis of $ts5^{-/-}$ mice, we generated $Cd44^{-/-}/ts5^{-/-}$ double knock-out mice. Examination of dermal wound healing in the double knockouts (Fig. 5*A*, *left panels*) clearly showed that the prolonged inflammation, ulceration, and lack of dermal regeneration characteristic of the $ts5^{-/-}$ mice (Fig. 1*B*) was not present. At the histological level, the cell aggregates and the disorganized collagen network seen in $ts5^{-/-}$ mice (Fig. 1*B*) were also absent (Fig. 5*A* and supplemental Fig. S1), supporting a central role for CD44 in the formation of the aggregates seen in $ts5^{-/-}$ mice. CD44 ablation alone resulted in a normal macroscopic wound healing process (Fig. 5*B*), with a complete restoration of the dermal collagen fiber network (Fig. 5*B* and supplemental Fig. S1) similar to that seen in wild types (Fig. 1*A* and supplemental Fig. S1). It was noted (Fig. 5), however, that the dermal thickness in mice lacking CD44 ($Cd44^{-/-}$ and $Cd44^{-/-}/ts5^{-/-}$) was about 100–150 μm, which is about 50% that in WT or single $ts5^{-/-}$ mice (250–300 μm). In addition, in all $Cd44^{-/-}$ mice the regeneration of hair follicles and hair growth was much reduced (Fig. 5, *A* and *B*). This is in agreement with other studies on dermal repair in $Cd44^{-/-}$ mice (39), which showed that CD44-HA binding has a function in promoting epithelioid/keratinocyte differentiation and is important for maintaining dermal barrier function.

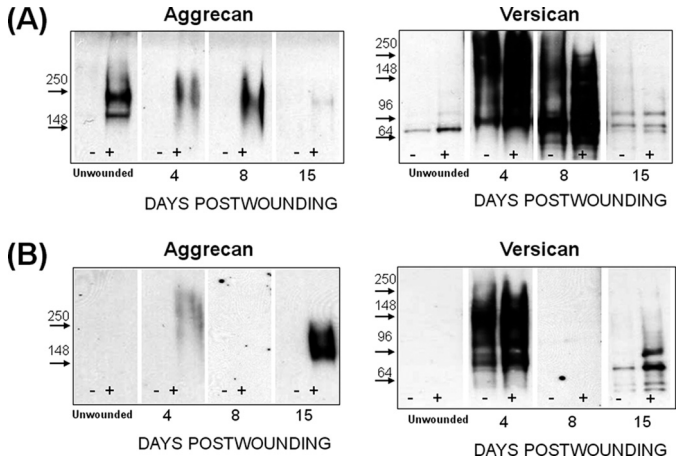

FIGURE 6. **Aggrecan and versican deposition in regenerating skin of $Cd44^{-/-};ts5^{-/-}$ (*A*) and $Cd44^{-/-}$ (*B*) mice.** Proteoglycans were prepared for Western analysis with anti-aggrecan (αDLS) and with anti-versican V1 (Ab1033). Each lane was loaded with 20% of the proteoglycan-rich fraction isolated from the four wound sites combined from one mouse. Samples loaded without and with chondroitinase ABC digestion are marked − and +, respectively. Images separated by *dividing lines* were from different parts of the same gel.

A pivotal role for CD44 in the accumulation of dermal aggrecan was supported by Western analysis (Fig. 6*A*), which showed that the wound sites of both CD44-deficient genotypes contained very little of this proteoglycan relative to either WT or $ts5^{-/-}$. Conversely, the increase in versican content during the granulation phase seen in $ts5^{-/-}$ mice (Fig. 2*B* and supplemental Fig. S3) was not eliminated by CD44 ablation (Fig. 6*A*), suggesting that versican deposition during this phase occurs without CD44. Furthermore, the persistent accumulation seen in

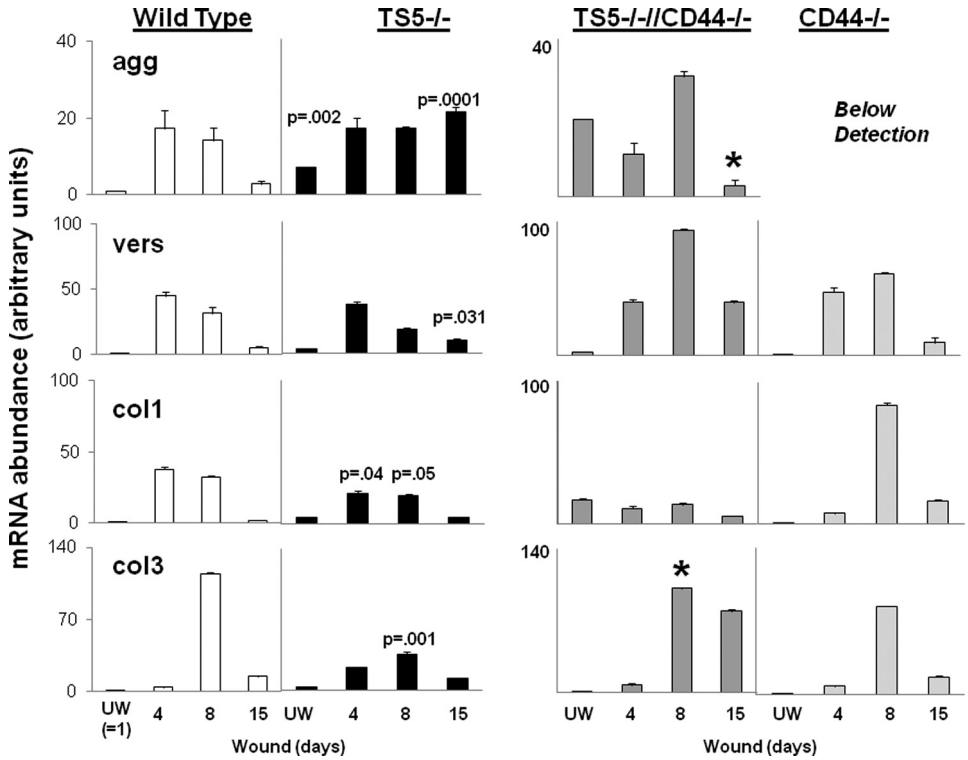

FIGURE 7. **Quantitative PCR of matrix gene expression in unwounded and wounded skin from WT, *ts5*$^{-/-}$, *ts5*$^{-/-}$/*Cd44*$^{-/-}$, and *Cd44*$^{-/-}$ mice.** RNA preparation and PCRs for aggrecan (*agg*), versican (*vers*) V1, col1a, and col3a transcript abundance were performed as described under "Experimental Procedures." Data for wounded tissue (at day 4 = granulation tissue; day 8 = contraction, and day 15 = dermal regeneration) are expressed as mRNA abundance (arbitrary units) relative to the unwounded (*UW*) wild type value that was set at unity. Each data point represents the mean ± S.D. of triplicate assays from three individual mice. See also supplemental Table 1 for basal level expression of all genes in all mice lines. *Asterisk* indicates the restoration of gene expression to WT values.

ts5$^{-/-}$ mice through day 8 (Fig. 2*A*) also occurred without CD44 (Fig. 6*A*). Nonetheless, the *ts5*$^{-/-}$/*Cd44*$^{-/-}$ mice were able to contract the wound and regenerate the dermal structure. We therefore conclude that in the absence of *ts5* it is the accumulation of aggrecan, but not versican, that is responsible for the aberrant healing response.

Aggrecan Gene Expression Is Enhanced in ts5$^{-/-}$ *Mice, Both in Unwounded Skin and Late Stage Healing*—To confirm Western and immunohistochemical detection of aggrecan and versican, we determined mRNA transcript abundance of the proteoglycans as well as the major dermal collagens, col1 and col3, in unwounded skin and at 4, 8, and 15 days post-wounding. Quantitative PCR was done on tissue taken from all four genotypes, and the data are expressed as mRNA abundance relative to the unwounded WT value (see "Experimental Procedures" and the figure legends for explanation). In WT mice (Fig. 7, *left column*), the transcript abundance was increased ~20-fold for aggrecan, ~40-fold for versican, and ~40-fold for col1 by day 4. Transcripts for *col3* were elevated slightly by day 4 but ~110-fold by day 8. All four transcripts returned to near unwounded levels by day 15. These transcript changes are consistent with a normal healing response to dermal wounding (41).

In *ts5*$^{-/-}$ mice, the changes in transcript abundance for *vers*, *col1*, and *col3* were similar to WT, except that the peak for col3 on day 8 was much reduced ($p = 0.001$). Most notably, the abundance of *agg* transcript was increased about 7-fold over WT in unwounded skin ($p = 0.002$), and it remained at an elevated level (about 20-fold) to day 15 ($p = 0.0001$).

Concomitant ablation of CD44 in *ts5*$^{-/-}$ mice caused general increases in *vers* and *col3* abundance on days 8 and 15 (which is the period of wound contraction and dermal fibrogenesis) but a reduction in *col1* ($p = 0.04$). Also, the *agg* abundance was somewhat higher than in *ts5*$^{-/-}$ alone, but in contrast it was normalized by day 15. For wounds in single *Cd44*$^{-/-}$ mice, the maximum increase in transcript abundance for *vers*, *col1*, and *col3* was at day 8 where *vers* message was increased ~50-fold, *col1* ~80-fold, and *col3* ~85-fold. The failure to detect *agg* mRNA in *Cd44*$^{-/-}$ skin both unwounded and at days 4, 8, and 15 post-wounding suggests that aggrecan synthesis is exceedingly low (Fig. 6*B*). The low level of aggrecan core detected in extracts of wounds at day 4 and 15 could, however, have been synthesized and deposited at intervals during days 1–3 and 9–14. This is because the mRNA levels were assayed only at days 4, 8, and 15, and *agg* mRNA may have been present during the intervening periods.

Expression of tgfβ1, alk1, alk5 and tgfβ1RII Are Modulated in Response to Dermal Wounding in All Genotypes—Because TGFβ1-mediated activation of genes such as *col1* and *col3* is considered to play a central role in successful dermal repair (41, 42), we next examined the effects of genotype on transcript abundance for tgfβ1, alk1, alk5, and tgfβ1RII in unwounded skin and on days 4, 8, and 15 post-wounding (Fig. 8). In WT mice, all genes were low in unwounded skin, and each was activated between 2.5-fold (alk1) and 10-fold (tgfb1) by wounding. In each case the greatest increase was on day 8 followed by a decrease at day 15.

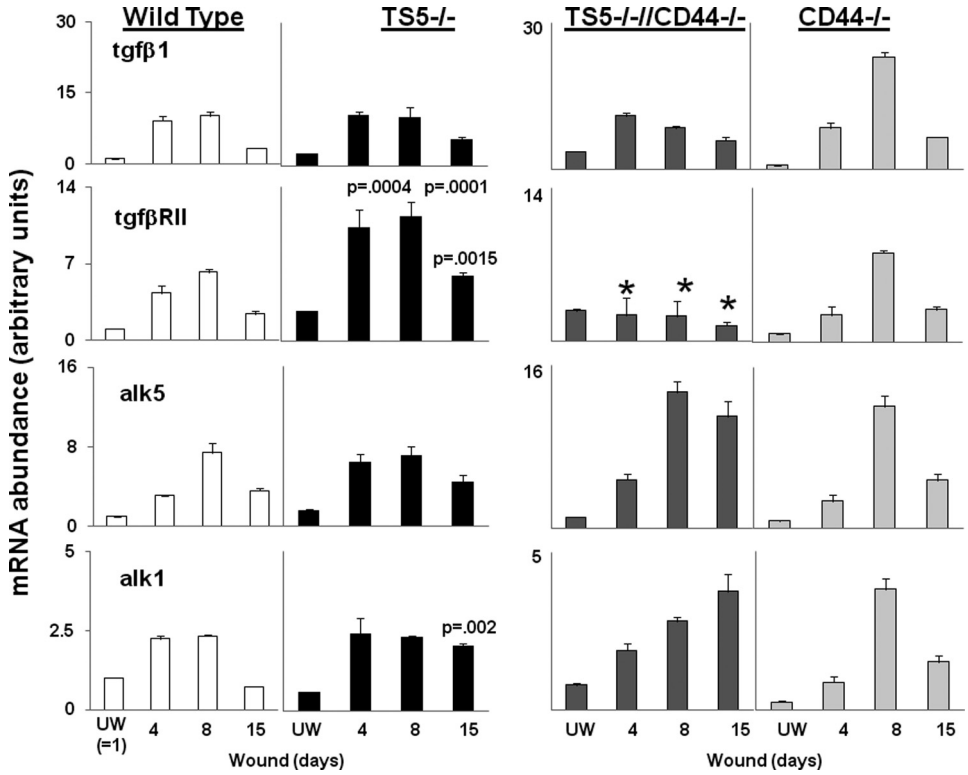

FIGURE 8. **Quantitative PCR for transcript abundance of tgfβ1, alk1, alk5, and tgfβ1RII in unwounded and wounded skin from WT, *ts5*$^{-/-}$, *ts5*$^{-/-}$/*Cd44*$^{-/-}$, and *Cd44*$^{-/-}$ mice.** RNA preparation and PCRs for transcript abundance was performed as described under "Experimental Procedures." Data for wounded tissue (at day 4 = granulation tissue; day 8 = contraction; and day 15 = dermal regeneration) are expressed as mRNA abundance (arbitrary units) relative to the unwounded (*UW*) wild type value, which was set at unity. Each data point represents the mean ± S.D. of triplicate assays from three individual mice. See also supplemental Table 1 for basal level expression of all genes in all mice lines. *Asterisk* indicates the restoration of gene expression to WT values.

ts5$^{-/-}$ mice also showed low levels of transcripts in unwounded skin, and after wounding, tgfβ1 and alk5 transcripts showed changes similar to WT. However, for tgfβ1RII, the increase after wounding was greater ($p = 0.0004$) and more prolonged than in WT, and for alk1, the abundance did not normalize ($p = 0.0013$) at day 15. The response pattern seen in *Cd44*$^{-/-}$;*ts5*$^{-/-}$ mice was similar to *ts5*$^{-/-}$ mice for tgfβ1. However, tgfβ1RII transcript abundance was much reduced at days 4, 8, and 15, and alk5 transcripts were higher on days 8 and 15, and alk1 transcripts were similar to *ts5*$^{-/-}$ wounds except for a further increase on day 15. In *Cd44*$^{-/-}$ mice, the change in abundance of all genes with time was similar to WT; however, the absolute values at day 8 were somewhat higher that WT. In summary, the most profound differences relative to WT were in the *ts5*$^{-/-}$ mice, which showed enhanced tgfβ1RII transcripts at all times and a lack of normalization of alk1 at day 15. Relative to *ts5*$^{-/-}$, concomitant ablation of *Cd44*$^{-/-}$ caused only a marked reduction of tgfβ1RII at all times.

TGFβ1-induced Smad Phosphorylation in Newborn Fibroblasts Is Markedly Different for Each Genotype—To examine whether the differences between genotypes in the post-wounding expression of TGFβ1 pathway components (Fig. 8) might be reflected in altered Smad phosphorylation, we analyzed TGFβ1-stimulated signaling responses in newborn fibroblasts. Fibroblast cultures were established from all four genotypes (as described under "Experimental Procedures") and treated with 10 ng/ml TGFβ1 (in DMEM + 0.1% FCS). Cells were lysed at timed intervals and analyzed by Western for phosphorylation of Smad2, Smad3C, and Smad1/5/8 (Fig. 9 and supplemental Fig. S7).

In WT cells, TGFβ1 induced robust phosphorylation of Smad2 between 30 and 120 min, an early increase (5–30 min) in pSmad3C, and a weak signal for pSmad1/5/8 at 60 min post-addition. In contrast, *ts5*$^{-/-}$ cells exposed to TGFβ1 did not phosphorylate Smad2 or Smad 3C significantly but responded with prolonged phosphorylation of Smad1/5/8. Furthermore, in the presence of TGFβ1, both *Cd44*$^{-/-}$ and *Cd44*$^{-/-}$/*ts5*$^{-/-}$ fibroblasts responded with early phosphorylation of Smad3C, much as seen in the WT cells, but this was followed by a further enhancement of the response at 60 and 120 min, which was not seen in WT cells. Moreover, fibroblasts from both *Cd44*$^{-/-}$ genotypes did not phosphorylate Smad2 or Smad1/5/8.

To analyze this further, we treated *ts5*$^{-/-}$ cells with Strep.hyase before addition of TGFβ1. The results showed that the treatment had released aggrecan from the cell-associated pool (supplemental Fig. S8), and this resulted in the production of pSmad2 and pSmad3C much as seen in the WT (Fig. 9). Taken together, these results show that in the newborn fibroblast cultures, TGFβ1-mediated Smad2 phosphorylation requires both CD44 and TS5. Smad1/5/8 phosphorylation requires CD44 in the absence of TS5, and Smad3C phosphorylation requires either the absence of pericellular aggrecan (as in both lines of *Cd44*$^{-/-}$ cells and after *Streptomyces* hyaluronidase treatment of *ts5*$^{-/-}$ cells) or its removal by TS5 (as in WT cells). In addition, the finding that full-length aggrecan, but not the G1-NITEGE product, was released from cell layers

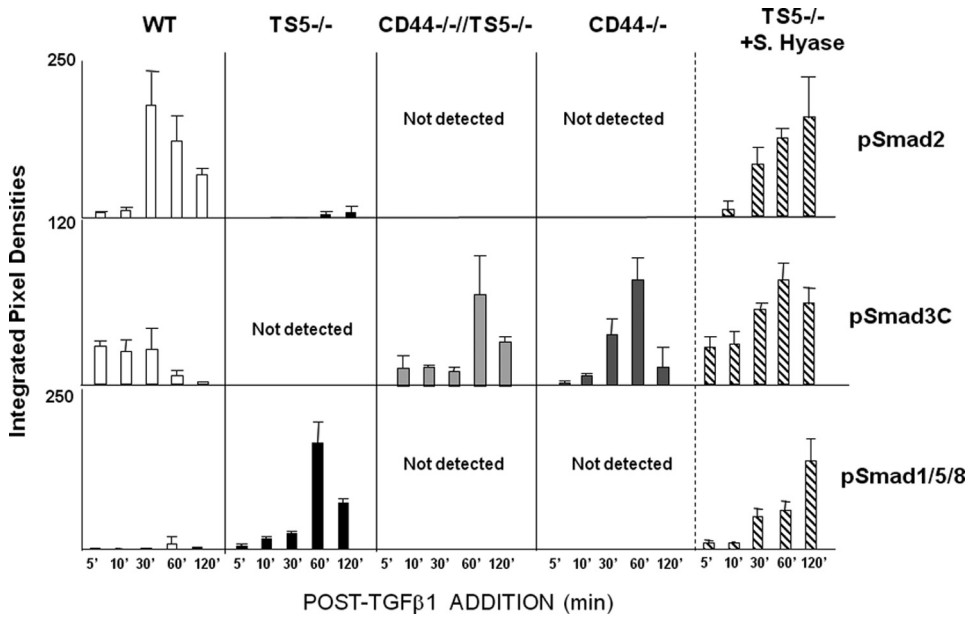

FIGURE 9. **Smad phosphorylation in newborn fibroblasts from WT, *ts5*$^{-/-}$, *ts5*$^{-/-}$/*Cd44*$^{-/-}$, and *Cd44*$^{-/-}$ + S.Hyase mice.** Fibroblast cultures from all genotypes were established and treated with TGFβ1 as described under "Experimental Procedures" (for basal matrix gene expression levels see supplemental Table 1). *ts5*$^{-/-}$ cells were also pretreated with *Streptomyces* hyaluronidase as described under "Experimental Procedures" before exposure to TGFβ1. Cell extracts were analyzed by Western for total and phosphorylated Smad2, Smad3C, and Smad1/5/8 (see typical gel images in supplemental Fig. S4). Data are expressed as integrated pixel density units for phosphorylated Smad proteins at 5–120 min post-TGFβ1 addition. Before the addition of TGFβ1, cells contained no detectable pSmad2 or pSmad 1/5/8. For two of the four WT cell preparations assayed, pSmad3C was detected even without addition of TGFβ1, and it represented about 25% that detected after 5 min. Data shown represent the mean ± S.D. for analyses of three separate cell preparations for each genotype.

(supplemental Fig. S8*B*) by Strep.hyase treatment suggests that the two are in separate pools of cell-surface HA.

DISCUSSION

We show here that aggrecan is a component of normal murine skin, where it is detected primarily in the ECM of the epidermis and also between the cell aggregates of the dermal papillae of hair follicles, much as previously described with human skin from normal individuals (7) and Hutchinson-Gilford progeria syndrome patients (43). In addition, we have shown that following dermal wounding in WT mice, aggrecan transcripts and protein become abundant during dermal regeneration (Figs. 2, 3, and 7). In this regard, it is relevant that aggrecan but not col2 (data not shown) is expressed during murine dermal wound healing and by newborn fibroblasts (supplemental Table S2). This suggests that aggrecan has an essential role independent of col2 expression in the condensation phase of fibroblast-based chondrogenic tissue constructs (44).

Aggrecan deposited in the granulation tissue of WT wounds is removed by day 8, a process that is essential for wound contraction and collagen deposition. This elimination of aggrecan between days 4 and 8 coincides with the highest expression levels for ADAMTS4 and TS5 (supplemental Fig. S5), which clearly suggests that ADAMTS-mediated aggrecanolysis is necessary for murine dermal wound healing. Our finding here that *ts5*$^{-/-}$ mice do not heal, but *ts4*$^{-/-}$ mice show essentially normal wound contracture and collagen fibrillogenesis (results not shown), suggests that TS5 alone is needed for this critical removal of aggrecan. In *ts5*$^{-/-}$ mice, aggrecan did not accumulate in the granulation phase (day 4) but instead during the time of contracture and dermal regeneration. Specifically, it is found in the ECM surrounding cell aggregates that are found throughout the nonhealing dermis (Fig. 4*C*). The aggrecan-rich cellular aggregates that arise in *ts5*$^{-/-}$ wounds resemble immature skin appendages such as hair follicles and sweat glands. Because their formation is also dependent on the presence of CD44 (Fig. 5), it can be assumed that aggrecan is a component of the cell-associated matrix of the progenitor cell populations present in such locations. This is further corroborated by the observation that fibroblastic cells in the regenerating dermis of *ts5*$^{-/-}$ mice have an aggrecan-rich cell-associated matrix that could "block" these cells from transitioning to mature collagen-producing and contracting fibroblasts.

To further examine the proposed central role of CD44 in supporting the *ts5*$^{-/-}$ phenotype, we determined the expression of cd44 in unwounded skin and at 4, 8, and 15 days post-wounding for both WT and *ts5*$^{-/-}$ mice (supplemental Fig. S5). This showed peak expression on day 4 in both phenotypes and normalization by day 15, which supports the idea that aggrecan accumulation in the *ts5*$^{-/-}$ skin is dependent on newly synthesized CD44. It should be noted here that because the abundance of cd44 transcript in unwounded *ts5*$^{-/-}$ skin was about 20-fold higher than for WT skin, the actual abundance of transcript at day 4 was similar for the two genotypes.

Unlike WT and *ts5*$^{-/-}$ mice, *Cd44*$^{-/-}$ and *Cd44*$^{-/-}$/*ts5*$^{-/-}$ mice did not accumulate aggrecan at any stage of the wound healing process, a finding that may be largely explained by defective retention of HA-bound aggrecan by CD44-deficient cells. In addition, in the *Cd44*$^{-/-}$ mice, the activity of TS5 is likely to accentuate the profibrotic gene activation in progenitor cells that populate the wound site (Fig. 7). Furthermore, a reduced number of pluripotent reparative cells in the wound

might further contribute to the wound healing phenotype in *Cd44*$^{-/-}$ mice. This would occur if such cells were dependent on CD44-mediated "homing" to the site, as has been reported for inflammatory cells and fibroblast progenitors (45, 46). Such a deficiency of progenitors in the absence of CD44 would also reduce the total number of cells capable of responding to TGFβ1 to restore the dermal collagen matrix. Thus, although the repair in both lines of *Cd44*$^{-/-}$ mice was sufficient for wound closure, the depth of both naive and repaired dermis in the *Cd44*-deficient genotypes was only about 50% that in WT or *ts5*$^{-/-}$ mice, which express *Cd44*. Furthermore, hair follicle development and hair growth itself in healed wounds were substantially impaired in both *Cd44*$^{-/-}$ genotypes (Fig. 5).

Whereas aggrecan turnover is clearly required for effective post-wound dermal restoration, analysis of the effects of *ts5* and *Cd44* on versican turnover does not suggest such a central role for this proteoglycan. For example, versican V1 accumulates in the wounds and cell clusters of *ts5*$^{-/-}$ mice (relative to WT), but it is removed by day 15. This suggests that it can be degraded by proteinases other than TS5 and that its accumulation at day 8 is unrelated to the nonhealing phenotype. Similarly, the temporal abundance of versican (at days 4, 6, and 8) is very similar in *ts5*$^{-/-}$ and *Cd44*$^{-/-}$/*ts5*$^{-/-}$ wounds; however, the *ts5*$^{-/-}$ wounds do not heal, whereas the double knock-out wounds heal effectively. An interesting aspect of the versican analysis (Fig. 2) is that the same pattern of accumulated fragments was seen in the *ts5*$^{-/-}$ knee following joint injury (30) suggesting that this versican fragment pattern is characteristic of soft tissue responses to wounding throughout the body in these mice. It is also significant that the accumulation of aggrecan, but not versican, in wounded skin is dependent on the presence of CD44, suggesting that the two are present in spatially and functionally distinct compartments of the cell-associated matrix, during the maturation of progenitor cells to mature fibroblasts.

Newborn skin fibroblast cultures (Fig. 9, supplemental Fig. S7, and supplemental Table S2) were used to model TGFβ1-induced dermal healing responses in all mouse genotypes. WT cells stimulated with TGFβ1 showed robust phosphorylation of Smad2 and Smad3C, consistent with activation of a profibrotic response (47, 48). Under these same conditions, *Cd44*$^{-/-}$/*ts5*$^{-/-}$ and *Cd44*$^{-/-}$ cells produced high levels of pSmad3C only, and this was accompanied by high expression of col3 (Fig. 7), consistent with a fibrotic scarring response (47, 49, 50). Most significantly, *ts5*$^{-/-}$ cells treated with TGFβ1 phosphorylated essentially only pSmad1/5/8, consistent with the loss of a fibrogenic response. It therefore appears that the nonhealing phenotype of *ts5*$^{-/-}$ mice can be largely attributed to an aberrant response of dermal fibroblasts and their progenitors to TGFβ1, a response that leads to dermal aggrecan accumulation. In addition, and most significantly, the response is completely dependent on the expression of *Cd44* by the same cells, and the lack of Smad2/3 signaling in *ts5*$^{-/-}$ cells can be restored by removal of the pericellular aggrecan with *Streptomyces* hyaluronidase (Fig. 9 and supplemental Fig. S8).

Based on the results presented here, a working model of the pathway by which fibroblast progenitors respond to TGFβ1 is provided in Fig. 10. In WT wounds, fibroblastic progenitor cells

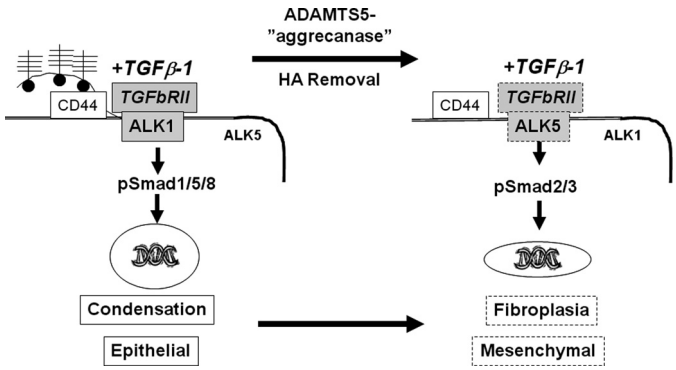

FIGURE 10. **Working model for regulation of TGFβ1 signaling in fibroblasts by hyaluronan-bound aggrecan, ADAMTS5, and CD44.** In the *ts5*$^{-/-}$ genotype (*left*), aggrecan is retained on CD44-bound HA and continues to accumulate due to the absence of TS5. This promotes binding of TGFβ1 to TGFβRII/ALK-1 leading to Smad1/5/8 phosphorylation, which promotes further commitment of target cells to an epithelioid/aggregating phenotype. Conversely, in WT and *Cd44*$^{-/-}$ cells (*right*), removal of aggrecan-HA complexes favors association of TGFβ1-TGFβRII with ALK5 resulting in robust Smad2/3 phosphorylation and expression of a fibroblastic/contractile phenotype.

are stimulated by anabolic growth factors in the granulation tissue environment (for example, EGF, IGF1, PDGF, or bone morphogenic proteins (51)) to produce aggrecan and hyaluronan, which after secretion form cell-associated aggregates with CD44. In this location, aggrecan is readily degraded by TS5, which is also being highly expressed at this time (supplemental Fig. S5). We suggest that this TS5-mediated removal of the chondroitin sulfate-rich region of aggrecan alters the charge environment of the cell-associated ECM (because of the loss of negatively charged sulfate) which, by an unknown mechanism, promotes binding of the TGFβ1·TGFβRII complex to ALK5 rather than to ALK1. This in turn promotes phosphorylation of Smad2/3, resulting in a fibrogenic response.

In the absence of TS5 (*left side* of Fig. 10), aggrecan is retained on CD44-bound HA and continues to accumulate due to the absence of the critical aggrecanase, which in this process must be TS5. We propose that the resulting aggrecan-rich and negatively charged pericellular ECM blocks the association of the TGFβ1·TGFβRII complex with ALK5. In the absence of such ALK5 binding, the TGFβ1·TGFβRII complex associates instead with available ALK1, leading to Smad1/5/8 phosphorylation; this in turn maintains a TGFβ1-responsive and epithelioid/aggregating phenotype throughout the regenerating dermis. *In vivo* support for the central role of ALK1 in this response is provided by the finding that in both *ts5*$^{-/-}$ genotypes, alk1 expression remained high during the dermal contraction and regeneration phase, whereas in WT skin it returned to base line (Fig. 8). Moreover, a screen of TGFβ1-stimulated genes in fibroblasts showed a 3-fold enhancement of alk1 in *ts5*$^{-/-}$ relative to WT.[3]

Finally, in both *Cd44*$^{-/-}$ mouse lines, the newly secreted aggrecan will not be retained in the pericellular space due to the absence of CD44-bound HA. The hypothetical scheme (Fig. 10) predicts that this will result in the association of TGFβ1·TGFβRII with ALK5 and fibrotic gene activation, resulting in a rapid fibroblastic dermal repair, but with no ref-

[3] D. Gorski and A. Plaas, unpublished data.

ormation of hair follicles and appendages that would require a continuous epithelioid/condensation response. These model predictions were indeed confirmed on histology of the repaired wounds in these mice (Fig. 5).

In summary, this study confirms and extends our studies on the need for TS5 activity in the repair of fibrous tissues. In keeping with this, we have shown (30) that treadmill-induced injury to TGFβ1-treated knee joints in wild type mice results in extensive fibrosis of the synovial lining and articular cartilage surface, leading to osteoarthritic changes in the whole joint. By comparison, in the strain of $ts5^{-/-}$ mice used for this study, no fibrosis was observed, but chondrogenesis and cartilage deposition occurred at the articular surface. Furthermore, biochemical and biomechanical analyses of murine tendons and ligaments (53–55) has shown that in $ts5^{-/-}$ mice there is an accumulation of intact aggrecan around chondroid cell clusters within the collagenous matrix, which leads to a change in collagen fibril structure and a loss of tensile properties. Particularly interesting is the finding in Achilles tendon that the lowest tensile strength, which is characterized by tendon rupture under tension, coincides with the region of highest aggrecan concentration.

Finally, these studies provide mechanistic support for the idea that TS5 has unique functional properties that distinguish it from other aggrecanases. Thus, by degrading pericellularly localized aggrecan, it appears to maintain pro-fibrotic TGFβ1 signaling in fibroblastic cells. It is likely that this unique function of TS5 is related to its confinement to the HA-rich pericellular matrix of cells in nonhealing ligaments (31) and in the superficial layer of articular cartilage (33).

REFERENCES

1. Schrementi, M. E., Ferreira, A. M., Zender, C., and DiPietro, L. A. (2008) *Wound Repair Regen.* **16,** 80–86
2. Nurden, A. T., Nurden, P., Sanchez, M., Andia, I., and Anitua, E. (2008) *Front. Biosci.* **13,** 3532–3548
3. Fathke, C., Wilson, L., Hutter, J., Kapoor, V., Smith, A., Hocking, A., and Isik, F. (2004) *Stem Cells* **22,** 812–822
4. Epstein, E. H., Jr., and Munderloh, N. H. (1978) *J. Biol. Chem.* **253,** 1336–1337
5. Carrino, D. A., Onnerfjord, P., Sandy, J. D., Cs-Szabo, G., Scott, P. G., Sorrell, J. M., Heinegård, D., and Caplan, A. I. (2003) *J. Biol. Chem.* **278,** 17566–17572
6. Tammi, R., Ripellino, J. A., Margolis, R. U., and Tammi, M. (1988) *J. Invest. Dermatol.* **90,** 412–414
7. Malgouries, S., Thibaut, S., and Bernard, B. A. (2008) *Br. J. Dermatol.* **158,** 234–242
8. Toriseva, M., and Kähäri, V. M. (2009) *Cell. Mol. Life Sci.* **66,** 203–224
9. Moses, M. A., Marikovsky, M., Harper, J. W., Vogt, P., Eriksson, E., Klagsbrun, M., and Langer, R. (1996) *J. Cell. Biochem.* **60,** 379–386
10. Plaas, A. H., and Sandy, J. D. (1993) *Matrix* **13,** 135–147
11. Kenagy, R. D., Plaas, A. H., and Wight, T. N. (2006) *Trends Cardiovasc. Med.* **16,** 209–215
12. Kenagy, R. D., Fischer, J. W., Lara, S., Sandy, J. D., Clowes, A. W., and Wight, T. N. (2005) *J. Histochem. Cytochem.* **53,** 131–140
13. Lemons, M. L., Sandy, J. D., Anderson, D. K., and Howland, D. R. (2001) *J. Neurosci.* **21,** 4772–4781
14. Wilson, C. G., Vanderploeg, E. J., Zuo, F., Sandy, J. D., and Levenston, M. E. (2009) *Arthritis Res. Ther.* **11,** R173
15. Lemke, A. K., Sandy, J. D., Voigt, H., Dreier, R., Lee, J. H., Grodzinsky, A. J., Mentlein, R., Fay, J., Schünke, M., and Kurz, B. (2010) *Cell Tissue Res.* **340,** 179–188
16. Patel, K. P., Sandy, J. D., Akeda, K., Miyamoto, K., Chujo, T., An, H. S., and Masuda, K. (2007) *Spine* **32,** 2596–2603
17. Voros, G., Sandy, J. D., Collen, D., and Lijnen, H. R. (2006) *Biochim. Biophys. Acta* **1760,** 1837–1844
18. Matthews, R. T., Gary, S. C., Zerillo, C., Pratta, M., Solomon, K., Arner, E. C., and Hockfield, S. (2000) *J. Biol. Chem.* **275,** 22695–22703
19. Tammi, R., Säämänen, A. M., Maibach, H. I., and Tammi, M. (1991) *J. Invest. Dermatol.* **97,** 126–130
20. Li, L., Heldin, C. H., and Heldin, P. (2006) *J. Biol. Chem.* **281,** 26512–26519
21. Yu, Q., and Stamenkovic, I. (2000) *Genes Dev.* **14,** 163–176
22. Hamilton, S. R., Fard, S. F., Paiwand, F. F., Tolg, C., Veiseh, M., Wang, C., McCarthy, J. B., Bissell, M. J., Koropatnick, J., and Turley, E. A. (2007) *J. Biol. Chem.* **282,** 16667–16680
23. Tolg, C., Hamilton, S. R., Nakrieko, K. A., Kooshesh, F., Walton, P., McCarthy, J. B., Bissell, M. J., and Turley, E. A. (2006) *J. Cell Biol.* **175,** 1017–1028
24. Meran, S., Thomas, D. W., Stephens, P., Enoch, S., Martin, J., Steadman, R., and Phillips, A. O. (2008) *J. Biol. Chem.* **283,** 6530–6545
25. David-Raoudi, M., Tranchepain, F., Deschrevel, B., Vincent, J. C., Bogdanowicz, P., Boumediene, K., and Pujol, J. P. (2008) *Wound Repair Regen.* **16,** 274–287
26. Prud'homme, G. J. (2007) *Lab. Invest.* **87,** 1077–1091
27. Saed, G. M., Kruger, M., and Diamond, M. P. (2004) *Wound Repair Regen.* **12,** 557–564
28. Mori, Y., Ishida, W., Bhattacharyya, S., Li, Y., Platanias, L. C., and Varga, J. (2004) *Arthritis Rheum.* **50,** 4008–4021
29. Chen, Y., Shi-wen, X., Eastwood, M., Black, C. M., Denton, C. P., Leask, A., and Abraham, D. J. (2006) *Arthritis Rheum.* **54,** 1309–1316
30. Li, J., Anemaet, W., Diaz, M. A., Buchanan, S., Tortorella, M., Malfait, A. M., Mikecz, K., Sandy, J. D., and Plaas, A. (2011) *J. Orthop. Res.* **29,** 516–522
31. Plaas, A., Sandy, J. D., Liu, H., Diaz, M. A., Schenkman, D., Magnus, R. P., Bolam-Bretl, C., Kopesky, P. W., Wang, V. M., and Galante, J. O. (2011) *J. Orthop. Res.* **29,** 900–906
32. Malfait, A. M., Ritchie, J., Gil, A. S., Austin, J. S., Hartke, J., Qin, W., Tortorella, M. D., and Mogil, J. S. (2010) *Osteoarthritis Cartilage* **18,** 572–580
33. Plaas, A., Osborn, B., Yoshihara, Y., Bai, Y., Bloom, T., Nelson, F., Mikecz, K., and Sandy, J. D. (2007) *Osteoarthritis Cartilage* **15,** 719–734
34. Derwin, K. A., Soslowsky, L. J., Kimura, J. H., and Plaas, A. H. (2001) *J. Orthop. Res.* **19,** 269–277
35. Plaas, A. H., Wong-Palms, S., Roughley, P. J., Midura, R. J., and Hascall, V. C. (1997) *J. Biol. Chem.* **272,** 20603–20610
36. Deleted in proof
37. Sandy, J., Westling, J., Kenagy, R. D., Iruela-Arispe, M. L., Verscharen, C., Rodriguez-Mazaneque, J. C., Zimmermann, D. R., Lemire, J. M., Fischer, J. W., Wight, T. N., and Clowes, A. W. (2001) *J. Biol. Chem.* **276,** 13372–13378
38. Lichti, U., Anders, J., and Yuspa, S. H. (2008) *Nat. Protoc.* **3,** 799–810
39. Bourguignon, L. Y., Ramez, M., Gilad, E., Singleton, P. A., Man, M. Q., Crumrine, D. A., Elias, P. M., and Feingold, K. R. (2006) *J. Invest. Dermatol.* **126,** 1356–1365
40. Knudson, C. B., and Toole, B. P. (1987) *Dev. Biol.* **124,** 82–90
41. Klass, B. R., Grobbelaar, A. O., and Rolfe, K. J. (2009) *Postgrad. Med. J.* **85,** 9–14
42. Wang, X. J., Han, G., Owens, P., Siddiqui, Y., and Li, A. G. (2006) *J. Investig. Dermatol. Symp. Proc.* **11,** 112–117
43. Lemire, J. M., Patis, C., Gordon, L. B., Sandy, J. D., Toole, B. P., and Weiss, A. S. (2010) *Mech. Ageing Dev.* **127,** 660–669
44. Arufe, M. C., Fuente, A. D., Fuentes, I., de Toro, F. J., and Blanco, F. J. (2010) *J. Cell. Biochem.* **111,** 834–845
45. Huebener, P., Abou-Khamis, T., Zymek, P., Bujak, M., Ying, X., Chatila, K., Haudek, S., Thakker, G., and Frangogiannis, N. G. (2008) *J. Immunol.* **180,** 2625–2633
46. Teder, P., Vandivier, R. W., Jiang, D., Liang, J., Cohn, L., Puré, E., Henson, P. M., and Noble, P. W. (2002) *Science* **296,** 155–158
47. Meng, X. M., Huang, X. R., Chung, A. C., Qin, W., Shao, X., Igarashi, P., Ju, W., Bottinger, E. P., and Lan, H. Y. (2010) *J. Am. Soc. Nephrol.* **21,** 1477–1487

48. Brown, K. A., Pietenpol, J. A., and Moses, H. L. (2007) *J. Cell. Biochem.* **101,** 9–33
49. Wang, Z., Gao, Z., Shi, Y., Sun, Y., Lin, Z., Jiang, H., Hou, T., Wang, Q., Yuan, X., Zhu, X., Wu, H., and Jin, Y. (2007) *J. Plast. Reconstr. Aesthet. Surg.* **60,** 1193–1199
50. Sumiyoshi, K., Nakao, A., Setoguchi, Y., Okumura, K., Tsuboi, R., and Ogawa, H. (2003) *Br. J. Dermatol.* **149,** 464–470
51. Barrientos, S., Stojadinovic, O., Golinko, M. S., Brem, H., and Tomic-Canic, M. (2008) *Wound Repair Regen.* **16,** 585–601
52. Pfaffl, M. W. (2001) *Nucleic Acids Res.* **29,** e45
53. Bell, R. M., Sandy, J. D., Malfait, A. M., Plaas, A. H., and Wang, V. M. (2010) *Trans. Orthop. Res. Soc.* **35,** 1098
54. Bell, R. M., Sandy, J. D., Plaas, A. H., and Wang, V. M. (2009) *Trans. Orthop. Res. Soc.* **34,** 1399
55. Bell, R. M., Thakore, R., Sandy, J. D., Malfait, A. M., Plaas, A. H., and Wang, V. M. (2010) *Trans. Orthop. Res. Soc.* **35,** 276